International Journal of Pharmacology

ISSN 1811-7775

science alert

ansinet
Asian Network for Scientific Information

OPEN ACCESS International Journal of Pharmacology

ISSN 1811-7775
DOI: 10.3923/ijp.2024.1063.1075

Research Article
Effects of Picroside Regulating the lncRNA-MALAT1/miR-21/PPAR Signaling Pathway in Fat Synthesis of Patients with Gestational Diabetes Mellitus

Dan Liu, Yang Zhang, Guxiang Zhang and Chengfang Xie

Department of Obstetrics and Gynecology, Changsha No. 4 Hospital, Changsha 410006, Hunan, China

Abstract

Background and Objective: The regulatory mechanism of picroside on fat synthesis in Gestational Diabetes Mellitus (GDM) remains unclear at present. This work investigated the regulatory effect of picroside on fat synthesis in patients with GDM and analyzed the roles of picroside in regulating the lncRNA-MALAT1, miR-21 and PPAR-γ signaling pathways (SPWs) in its effects on fat synthesis. **Materials and Methods:** Picroside was extracted and purified. Human subcutaneous adipocytes (3T3-L1) were divided into control (Ctrl), model (Mod) and picroside groups. Triglyceride (TG) and total cholesterol (TC) were detected and lncRNA-MALAT1 and miR-21 were measured. Protein levels of Peroxisome Proliferator-Activated Receptor Gamma (PPAR-γ), CCAAT/Enhancer-Binding Protein Alpha (C/EBP-α), etc., were determined. **Results:** The highest concentration of picroside extracted after 3 hrs using 95% ethanol was 279.25 mg/g. After purification with D201 macroporous adsorption resin, the mass fraction of picroside was 43.23%. In the Mod group, levels of TC, TG and lncRNA-MALAT1 were markedly elevated versus the Ctrl group ($p<0.05$). In picroside group, TC, TG and lncRNA-MALAT1 levels were superior to the Mod group ($p<0.05$). **Conclusion:** These findings indicated that picroside regulated fat synthesis in patients with GDM through the lncRNA-MALAT1/miR-21/PPAR-γ SPW.

Key words: Picroside, gestational diabetes mellitus, ncRNA-MALAT1, PPAR signaling pathway, fat synthesis

Citation: Liu, D., Y. Zhang, G. Zhang and C. Xie, 2024. Effects of picroside regulating the lncRNA-MALAT1/miR-21/PPAR signaling pathway in fat synthesis of patients with gestational diabetes mellitus. Int. J. Pharmacol., 20: 1063-1075.

Corresponding Author: Dan Liu, Department of Obstetrics and Gynecology, Changsha No. 4 Hospital, Changsha 410006, Hunan, China

Competing Interest: The authors have declared that no competing interest exists.

Data Availability: All relevant data are within the paper and its supporting information files.

INTRODUCTION

Gestational Diabetes Mellitus (GDM) is a transient hyperglycemia in the period of pregnancy and is among the most common pregnancy complications[1-3]. The GDM not only increases the risk of maternal conditions such as gestational hypertension and diabetes but also raises the risk of fetal malformations and neonatal hypoglycemia[4]. Currently, employed clinical interventions for GDM, including dietary control, physical exercise and insulin injections, face various limitations during implementation[5]. Aberrant fat synthesis is a crucial factor in the progression of GDM and is regulated by multiple molecular mechanisms, closely associated with insulin signaling pathways[6]. Chronic insulin resistance and abnormal insulin secretion are key features of GDM, although the precise regulatory mechanisms remain unclear[7]. The lncRNA-MALAT1 may be crucial in insulin signaling and glucose metabolism[8]. Additionally, MicroRNA-21(miR-21) is tightly linked to insulin secretion and insulin resistance[9].

Coptis chinensis, commonly known as Huang-Lian, is an extensively utilized medicinal herb in traditional Chinese medicine. It is known for its properties of clearing dampness, cooling blood, drying dampness and relieving infantile malnutrition. It is used to treat conditions such as bone-steaming fever, jaundice, cold and heat diarrhea, infantile malnutrition, spontaneous sweating, night sweats, hemorrhoids and abscesses[10,11]. Picroside is one of the active components extracted from the traditional herb *Coptis chinensis*. It exhibits significant anti-inflammatory effects, inhibiting the release of inflammatory mediators and the occurrence of inflammatory reactions. This potential therapeutic use has been explored for inflammation-related conditions such as intestinal inflammation and arthritis[12,13]. Research has indicated that picroside can inhibit tumor cell growth, induce apoptosis and inhibit metastasis. It also enhances the sensitivity to chemotherapy drugs, showing inhibitory effects on cancers like liver, breast and lung cancer[14]. Picroside has demonstrated blood glucose-lowering activity by increasing insulin sensitivity and promoting glucose utilization. It has been extensively studied and applied in treating GDM[15]. Picroside can improve insulin resistance, enhance insulin secretion and improve insulin signal transmission efficiency[16]. By inhibiting hepatic glycogen synthesis and increasing the expression of glucose transporter proteins in the liver, picroside can lower blood glucose levels[17]. Research results have indicated that picroside can also reduce lipid synthesis in fat cells and mitigate adipose tissue inflammation, thereby improving insulin resistance and metabolic abnormalities[18].

However, the regulatory mechanism of picroside on fat synthesis in GDM remains unclear. In this context, this work was developed focusing on the regulatory effect of picroside on fat synthesis in patients with GDM and further, exploring its potential molecular mechanisms. It was hypothesized that picroside may regulate the fat synthesis of patients with GDM through the lncRNA-MALAT1/miR-21/PPAR-γ signaling pathway (SPW). Meanwhile, this work focused on elucidating the role of picroside in modulating lncRNA-MALAT1, miR-21 and PPAR-γ SPW, to understand the effects of picroside on fat synthesis. Ultimately, this work was to yield new insights and potential targets in preventing and treating GDM.

MATERIALS AND METHODS

Study area: The study was conducted at the Changsha No. 4 Hospital from October, 2022 to July, 2023.

Methods for picroside crude extraction: The methodology outlined in Qin *et al.*[19] utilized the immersion method and organic solvent extraction to crudely extract picroside from the roots and rhizomes of *Coptis chinensis* (Anhui Bozhou Medicinal Market, China). The specific procedure was as follows. As 600 g of *Coptis chinensis* rhizomes were pulverized and coarse particles were removed by sieving through a 10-30 mesh screen. The sieved *Coptis chinensis* rhizomes were soaked in industrial alcohol for one week. The soaking solution was filtered and the collected filtrate was combined. The collected soaking solution was subjected to vacuum distillation using a rotary evaporator to recover ethanol. By controlling temperature and pressure, ethanol was evaporated to obtain concentrated *Coptis chinensis* total extract, which was then suspended in water to ensure thorough mixing. Subsequently, successive extractions were performed to obtain the petroleum ether fraction (1#), chloroform fraction (2#), ethyl acetate fraction (3#), n-butanol fraction (4#) and water-soluble fraction (5#) of the active components. The crude extraction process of picroside was illustrated in Fig. 1.

Methods for picroside extraction: Following the methodology described in Wang *et al.*[20], the Soxhlet extraction method was employed to further extract picroside from the crude extract. Six grams of picroside crude extract (PCE) was mixed with 3 to 9 times its weight of ethanol solution, with ethanol concentrations ranging from 55 to 95%. The extraction was carried out for 1 to 4 hrs, with 2 to 5 extraction cycles, until the solvent became colorless.

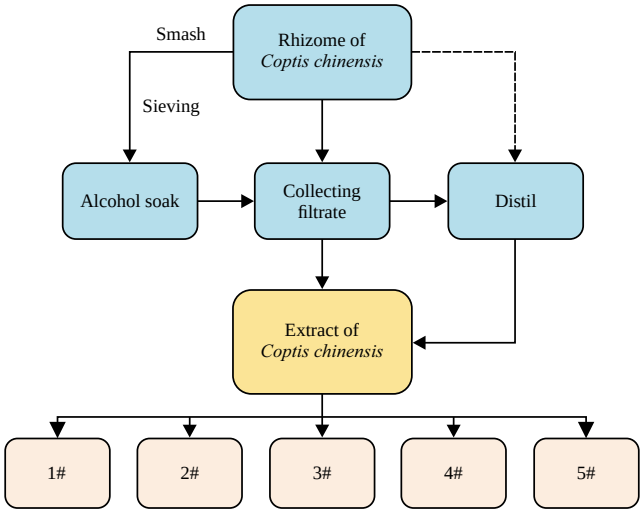

Fig. 1: Visualized presentation of picroside crude process

MPAR to purify picroside: The D101 macroporous resin (TianjiOuri BioTech Co., Ltd., China), NKA-9 macroporous adsorption resin (Tianjin Nankai University Chemical Plant, China), DB301 macroporous adsorption resin (Tianjin Ouri BioTech Co., Ltd., China), D3520, D201 and AB-8 macroporous adsorption resin (Tianjin University Chemical Plant, China), HPD100 macroporous adsorption resin (Cangzhou Baon Chemical Co., Ltd., China) underwent pretreatment. Then, 0.4 g of pretreated MPAR was weighed into a 50 mL conical flask, which was filled with 30 mL of *Coptis chinensis* extract. The samples were thoroughly adsorbed using an electric shaker at a frequency of 140 oscillations per minute for a continuous duration of 10 hrs. Subsequently, the mixture was filtered. The remaining concentration of picroside in the filtrate was determined using High-Performance Liquid Chromatography (HPLC) system (1260 Infinity model, Agilent Technologies, USA). The adsorption capacity of each resin at room temperature was calculated using the following Eq. 1:

$$A_C = \frac{C_1 - C_2}{W} \quad (1)$$

where, A_c represented the resin adsorption capacity, in mg/g, C_1 was the initial concentration, in mg/mL and C_2 was the remaining concentration, in mg/mL, v represented the solution volume, in mL and W stood for the resin weight, in g.

After achieving full adsorption, 30 mL of ethanol solutions with concentrations of 55, 65, 75, 85 and 95% were individually added to the resin. The mixtures were subjected to 10 hrs of oscillation, followed by filtration. The remaining concentration of picroside in the filtrate was determined using HPLC. The desorption rate of picroside from the macroporous resin was calculated using the following Eq. 2[21]:

$$D_r = \frac{D_C}{A_C} \quad (2)$$

where, A_c represented the resin adsorption capacity, in mg/g, D_r stood for the resin desorption rate, in percentage (%) and D_c referred to desorption, in mg/g.

Picroside detection: Ten milligrams of reference standard of picroside (China National Institutes for Food and Drug Control, China) and 5 mg of test samples were individually weighed and dissolved in water, then diluted to the respective concentrations. The HPLC was employed to quantify the amount of picroside in the extracts and purified products. Chromatographic column (Agilent Technologies, USA; Plus C18) with dimensions of 4.6×250 mm and a particle size (PS) of 5 µm was used. The mobile phase for the chromatographic column was a mixture of acetonitrile and water (in a volume ratio of 19:81). Detection was carried out at 264 nm. The injection volume was 10 µL and the flow rate was set at 1 mL/min, with the column temperature maintained at 30°C.

Culture, induction differentiation and grouping of 3T3-L1 cells: Human subcutaneous adipocytes (3T3-L1) were seeded onto a 6-well plate and cultured in Dulbecco's Modified Eagle Medium (DMEM) (Gibco, USA) complete medium containing 0.1% fetal bovine serum, 10 U/L penicillin and 10 U/L streptomycin. The 3T3-L1 cells from the 4th to 6th passages were used for induction and differentiation. Upon cell confluence, the medium was switched to DMEM complete medium containing 0.5 mmol/L isobutylmethylxanthine

(IBMX), 0.25 μmol/L dexamethasone and 1 mg/L insulin for induction and differentiation of 3T3-L1 cells. After 48 hrs of cultivation, the medium was continued with DMEM complete medium containing only 1 mg/L insulin and the cells were further cultured for approximately 13 days until over 90% of the cells had differentiated into mature adipocytes.

Based on different cell treatments, the cells were categorized into three groups: Control (Ctrl) group, model (Mod) group and picroside group. In Ctrl group, cells were treated with DMEM medium. In Mod group, cells were subjected to induction and differentiation treatment. In the picroside group, cells were induced and differentiated and then treated with 100 μL of purified picroside to achieve concentrations of 0.16, 0.48 and 1.44 mg/mL, respectively. Each group was composed of 6 replicates.

Detection of indicators related to fat synthesis: Triglyceride (TG) and total cholesterol (TC) contents in the 3T3-L1 cells were quantified using triglyceride and total cholesterol assay kit (Beijing ApplyGen Company, China). After adjusting the concentration to 6×10^5 cells/mL, they were seeded into a 6-well culture plate until they reached 80% confluence. After reaching this confluence, cells were treated according to the different group protocols. The culture medium was removed after a 24 hrs treatment period and cells were washed twice with pre-chilled PBS. Cells were then collected by centrifugation at 1,300 rpm for 15 min. The cell pellet was treated with TG cell lysis solution for 30 min and 10 μL of the lysate was transferred to a detection plate. Subsequently, 190 μL of a working solution was added and the plate was incubated at 37°C in the dark for 20 min. Absorbance at 570 nm was measured using a SpectraMax iD3 microplate reader (Zhejiang Meigu Biotechnology Co., Ltd., China) and TG and TC contents were calculated based on the absorbance values.

RT-qPCR method to detect expressions of cell factors: Expressions of lncRNA-MALAT1 and miR-21 in distinct groups of 3T3-L1 cells were assessed using the RT-qPCR method. Cells treated under different conditions were collected and treated with 1 mL of TRIzol reagent for cell lysis. Total RNA was extracted from the human 3T3-L1 cells using the TRIzol method. After assessing the extracted total RNA using agarose gel electrophoresis, reverse transcription was performed using a reverse transcription kit (Nanjing Shengxing Biotechnology Co., Ltd., China) with the following protocol: 37°C for 15 min, followed by 85°C for 5 sec. The GAPDH and U6 were used as internal references for lncRNA-MALAT1 and miR-21, respectively, to analyze their expression levels in the cells. Each reaction was performed in triplicate, with an annealing temperature of 60°C and an annealing time of 30 sec for 30 cycles. Furthermore, the $2^{-\Delta\Delta ct}$ method was utilized to calculate the levels of lncRNA-MALAT1 and miR-21 in the cells. The primer sequences for lncRNA-MALAT1, miR-21, GAPDH and U6 amplification were provided in Table 1.

Western blotting: Protein levels of PPAR-γ, C/EBP-α, FAS and ACC in the cells were determined using the western blotting method. Total proteins were extracted from the cells using RIPA solution. The protein concentration was quantified using the Bicinchoninic Acid kit (Shanghai Beyotime Biotechnology Co., Ltd., China). Proteins were separated using SDS-PAGE electrophoresis and transferred to a PVDF membrane. The membrane was blocked with 5% skim milk at room temperature for 2 hrs. Subsequently, diluted primary antibodies, including PPAR-γ (1:2000), C/EBP-α (1:2000), FAS (1:2000), ACC (1:2000) and β-actin (1:1000), were added and incubated overnight at 4°C. The primary antibody against the protein was purchased from Abcam (UK). The membrane was washed with TBST, followed by incubation with Horseradish Peroxidase-conjugated IgG secondary antibodies (1:8000) at room temperature for 1 hr. The secondary antibody against the protein was purchased from Signalway Antibody, USA. After washing the membrane with TBST, chemiluminescence assay kit (Shanghai Beyotime Biotechnology Co., Ltd., China) were used to visualize protein bands. The intensity of the target protein bands was quantified using ImageJ in a KETA GL fully automated gel imaging analysis system (Wealtec Corporation, USA).

Statistical analysis: All experimental data were presented as Mean±Standard Deviation or frequency (%) and analyzed using SPSS 22.0. For continuous variables, a t-test was employed for comparisons between two groups and One-way Analysis of Variance (ANOVA) was utilized for comparisons among multiple groups. The Chi-square test was adopted for categorical data. The $p<0.05$ was considered statistically significant.

Table 1: Primers sequences

Gene	Forward primer	Reverse primer
lncRNA-MALAT1	5'-TGGATTTCGTGGCCCCAGTGCTA-3'	5'-GCCACTGCTGTAGCCACTCA-3'
miR-21	5'- TTCATCCTGTTCTTCCTCGGCG -3'	5'- AGGTTACCAACAGAGTGTCTTG-3'
GAPDH	5'-AGTTCAACGGCACAGTCAAG-3'	5'-CAGCCTTCTCCATGGTGGTG-3'
U6	5'- GAGAGAAGCCGTCGTGT-3'	5'- TTGC-GAAGTGCTTAAACGCA-3'

RESULTS

Results of PCE: Firstly, the analysis of picroside content in different PSs of *Coptis chinensis* root was conducted, as presented in Fig. 2. As the PS increased, the content of picroside gradually increased. The picroside content was 6.76% for PSs of 10~15 mesh and it increased to 13.23% when the PS was in the range of 25~30 mesh. It can be observed that the best picroside extraction efficiency was achieved with a PS of 25~30 mesh. Hence, for subsequent experiments, PSs of 20~25 mesh were selected, corresponding to a picroside content of 11.62%.

With the yield of *Coptis chinensis* root as the reference (100%), the extraction yields of picroside in different solvents were calculated and the statistical results of different product weights and their corresponding picroside extraction yields were presented in Fig. 3. The total weight of *Coptis chinensis* crude extract was 224 g, corresponding to a picroside extraction yield of 37.33%. Among the various extraction solvents, the highest extraction yield was obtained with the n-butanol fraction (4#), reaching up to 17.67%. Based on these findings, we can infer that n-butanol is one of the most suitable solvents for the crude extraction of picroside. It can effectively extract picroside from the plant material and achieve a relatively high picroside extraction yield.

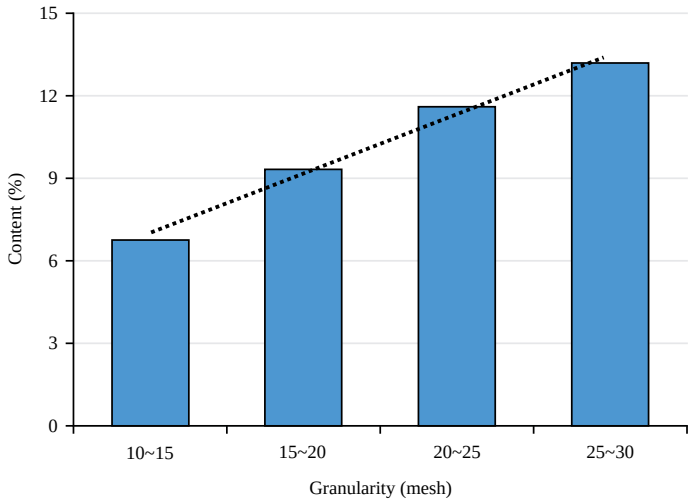

Fig. 2: Influences of PS on picroside content

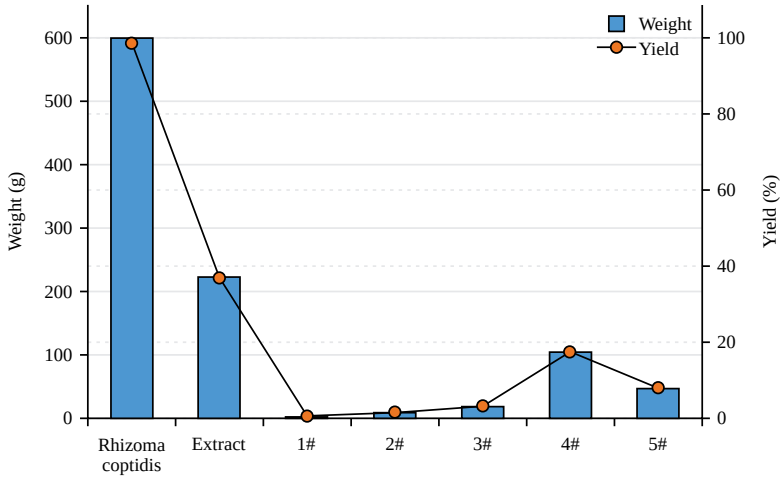

Fig. 3: Extraction results of picroside

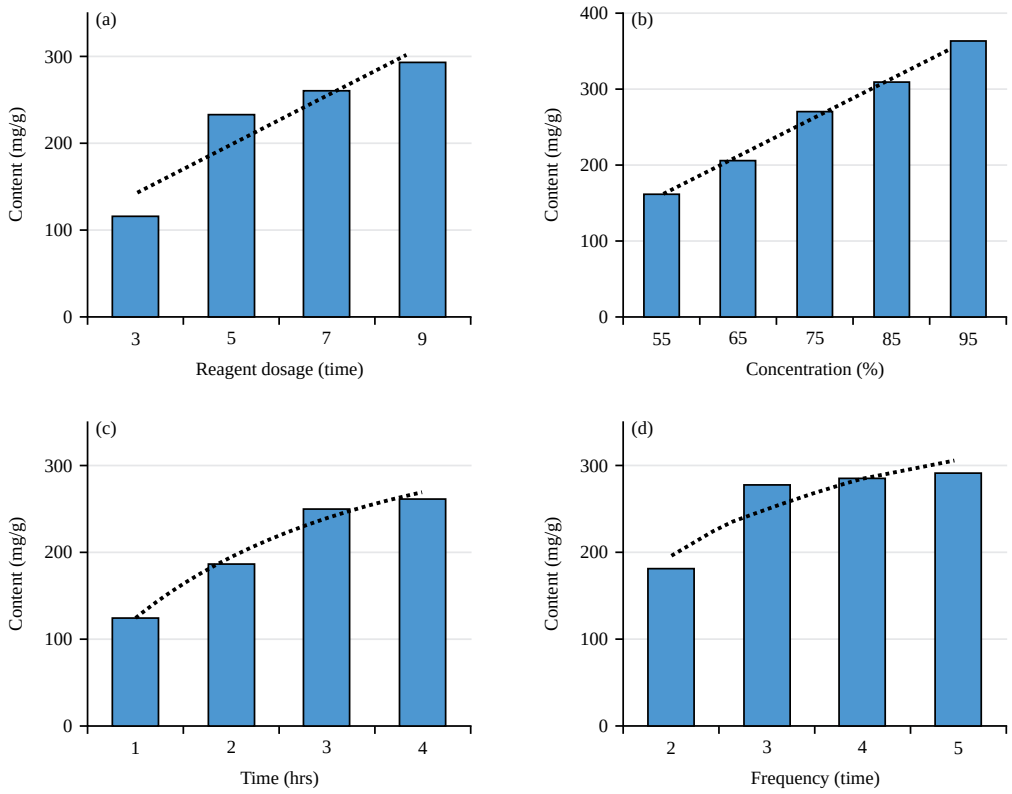

Fig. 4(a-d): Influencing factors of picroside extraction, (a) Solvent volume, (b) Ethanol concentration, (c) Extraction time and (d) Number of extractions

Influencing factors of picroside extraction: Figure 4 illustrated the effects of solvent volume, ethanol concentration, extraction time and number of extractions on the extraction of picroside. As both solvent volume and ethanol concentration increased, the extraction of picroside showed a noticeable upward trend. When the solvent volume was 9 times the sample weight, the highest picroside extraction was recorded at 294.52 mg/g (Fig. 4a). Similarly, with an ethanol concentration of 95%, the maximum picroside extraction reached 363.83 mg/g (Fig. 4b). Additionally, it was evident that the extraction of picroside initially increased and then stabilized with longer extraction times and higher numbers of extractions. At a 3 hrs extraction time, the picroside yield was 251.19 mg/g (Fig. 4c) and with 3 extraction cycles, the yield reached 279.25 mg/g (Fig. 4d). Further increasing the number of extractions did not greatly affect the picroside yield. These results indicated that increasing solvent volume and ethanol concentration enhanced the picroside extraction efficiency, while extending extraction time and conducting more extractions boost picroside yield, albeit with a saturation effect. Therefore, solvent volume at 9 times the sample weight, 95% ethanol concentration, 3 hrs extraction time and 3 hrs extraction cycles for picroside extraction were defined and employed in this work.

Results of picroside purification: The ability of different types of MPAR to purify picroside was evaluated from three aspects: Picroside mass fraction, picroside yield and picroside adsorption capacity. The statistical results were presented in Fig. 5. Variations in picroside mass fraction, yield and adsorption capacity were observed among different types of MPARs. Among them, D201 MPAR exhibited the highest performance in purifying picroside, followed by AB-8 MPAR (Fig. 5a-c). For D201 MPAR, the picroside mass fraction, yield and adsorption capacity were 43.23%, 20.30 g and 222.28 mg/g, respectively. For AB-8 MPAR, the corresponding values were 39.92%, 18.26 g and 210.49 mg/g, respectively.

Figure 6 illustrated the desorption rates of various types of MPARs at distinct ethanol concentrations. It was evident from the graph that both D201 and AB-8 MPARs exhibited higher desorption rates compared to other MPARs. Among them, D201 MPAR demonstrated the highest picroside desorption rate under different ethanol concentrations. With increasing ethanol concentration, the picroside desorption rate of D201 MPAR initially elevated and then declined. Specifically, when the ethanol was 55, 65, 75, 85 and 95%, the picroside desorption rates of D201 MPAR were 82.46, 98.25, 100.29, 99.18 and 97.39%, respectively.

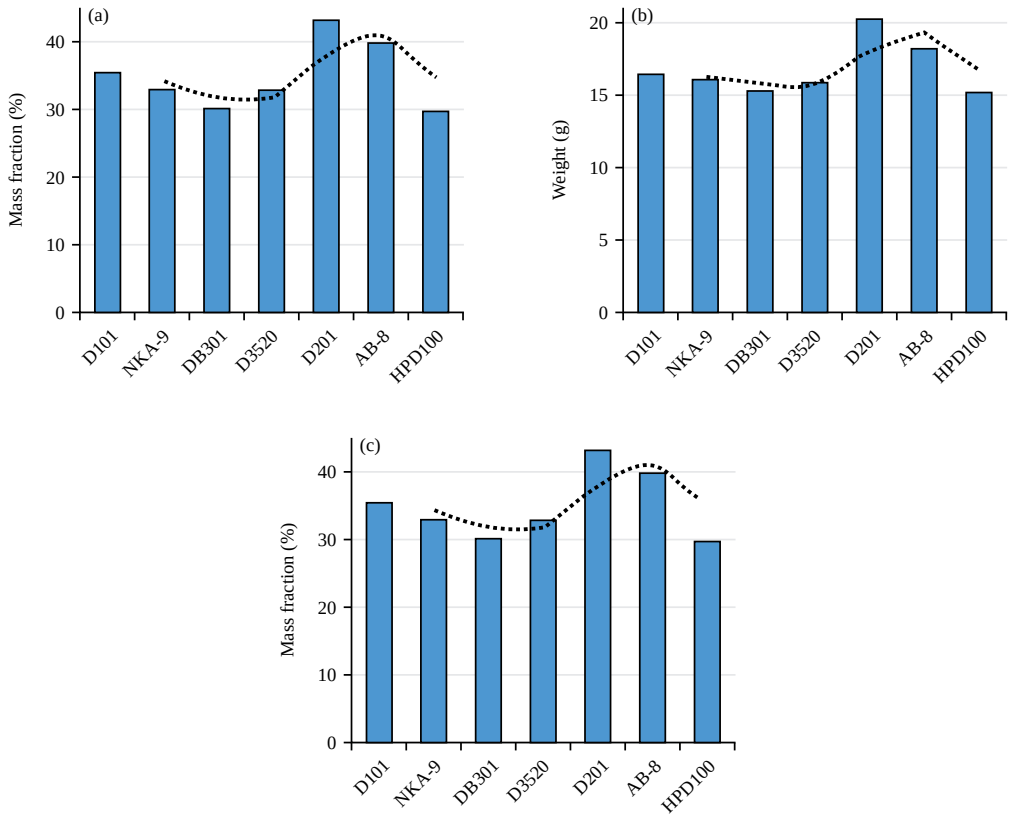

Fig. 5(a-c): Effects of different MPARs on picroside adsorption capacity, (a) Mass fraction, (b) Yield and (c) Adsorption capacity

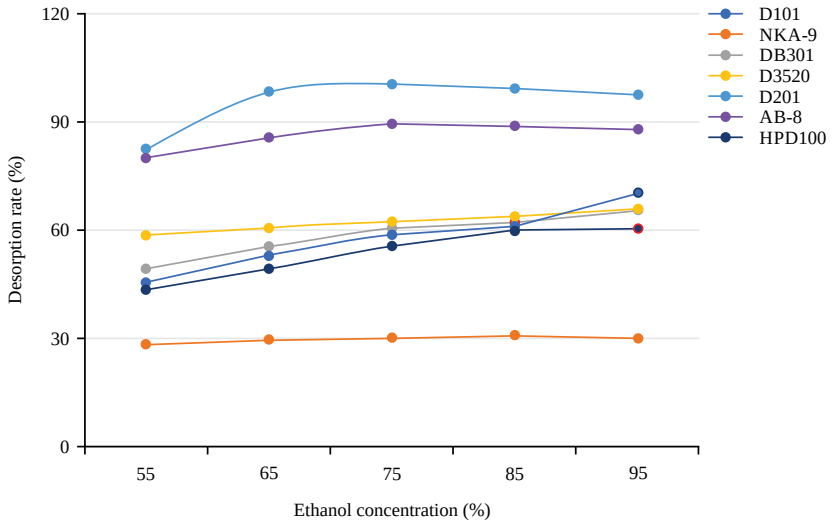

Fig. 6: Effects of MPARs on picroside desorption rate

Influences of picroside on TC and TG contents: Figure 7 illustrated the TC and TG levels in 3T3-L1 cells from different groups. In the Mod group, the TC content was elevated compared to the Ctrl group ($p<0.001$). The TC content in 3T3-L1 cells treated with 0.16 mg/mL picroside was higher than that in the Ctrl group ($p<0.01$), but lower than that in the Mod group ($p<0.05$). After treatment with 0.48 mg/mL picroside, the TC content in 3T3-L1 cells was higher than that in the Ctrl group ($p<0.05$), but significantly lower than that in the Mod group ($p<0.01$). In 3T3-L1 cells treated with

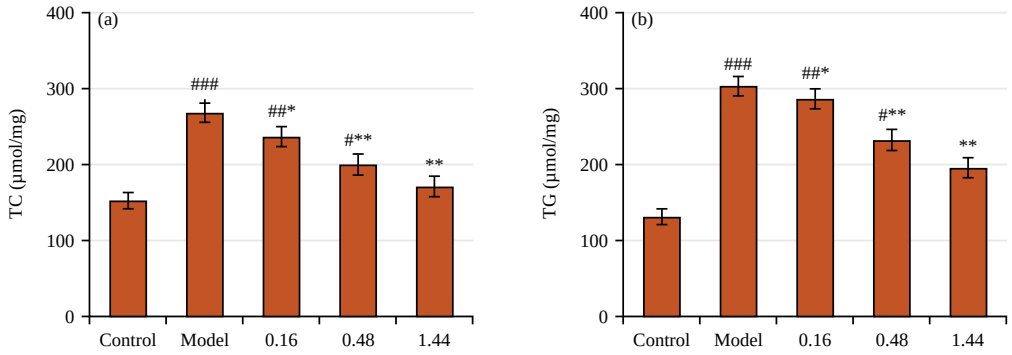

Fig. 7(a-b): Effects of picroside on (a) TC and (b) TG contents

#Compared with Ctrl group (p<0.05), ##Compared with Ctrl group (p<0.01), ###Compared with Ctrl group (p<0.001), *Compared with Mod group (p<0.05) and **Compared with Mod group (p<0.01)

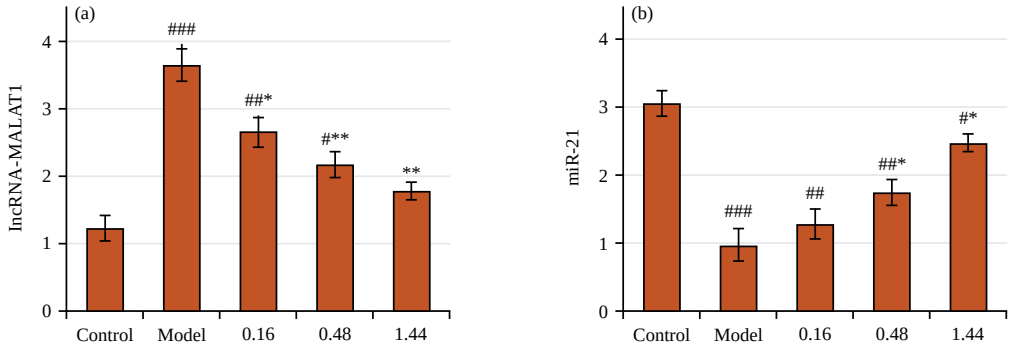

Fig. 8(a-b): Effects of picroside on (a) lncRNA-MALAT1 and (b) miR-21

#Compared with Ctrl group (p<0.05), ##Compared with Ctrl group (p<0.01), ###Compared with Ctrl group (p<0.001), *Compared with Mod group (p<0.05) and **Compared with Mod group (p<0.01)

1.44 mg/mL picroside, the TC content was lower than that in the Mod group (p<0.01) (Fig. 7a). Similarly, in the Mod group, the TG content was elevated compared to the Ctrl group (p<0.001). The TG content in 3T3-L1 cells treated with 0.16 mg/mL picroside was higher than that in the Ctrl group (p<0.01), but lower than that in the Mod group (p<0.05). After treatment with 0.48 mg/mL picroside, the TG content in 3T3-L1 cells was higher than that in the Ctrl group (p<0.05), but significantly lower than that in the Mod group (p<0.01). In 3T3-L1 cells treated with 1.44 mg/mL picroside, the TG content was lower than that in the Mod group (p<0.01) (Fig. 7b).

Effects of picroside on lncRNA-MALAT1 and miR-21: Figure 8a compared the lncRNA-MALAT1 in different 3T3-L1 cells groups. The Mod group exhibited sharply higher lncRNA-MALAT1 compared to Ctrl group. Treatment with picroside lead to a remarkable downregulation in lncRNA-MALAT1 based on that in Mod group (p<0.05), but it remained higher when comparing to Ctrl group (p<0.05).

Figure 8b compared the changes in miR-21 in 3T3-L1 cells from different groups. The Mod group showed decreased miR-21 and exhibited great difference with Ctrl group (p<0.05). Treatment with picroside leads to a remarkable increase in miR-21 expression and showed a visible difference to Mod group (p<0.05), while it remained lower when comparing with the Ctrl group (p<0.05).

Effects of picroside on protein levels of PPAR-γ SPW: The effects of picroside on PPAR-γ, C/EBP-α, FAS and ACC, as well as SPW, were presented in Fig. 9. In the Mod group, PPAR-γ decreased to Ctrl and picroside groups, showing obvious differences with p<0.001 and p<0.05, respectively. Protein levels of C/EBP-α, FAS and ACC in Mod group were all sharply lower and exhibited obvious differences with those in Ctrl group (p<0.05) (Fig. 9a-e) and those in picroside group showed an increase with observable differences to the levels in Mod group (p<0.05).

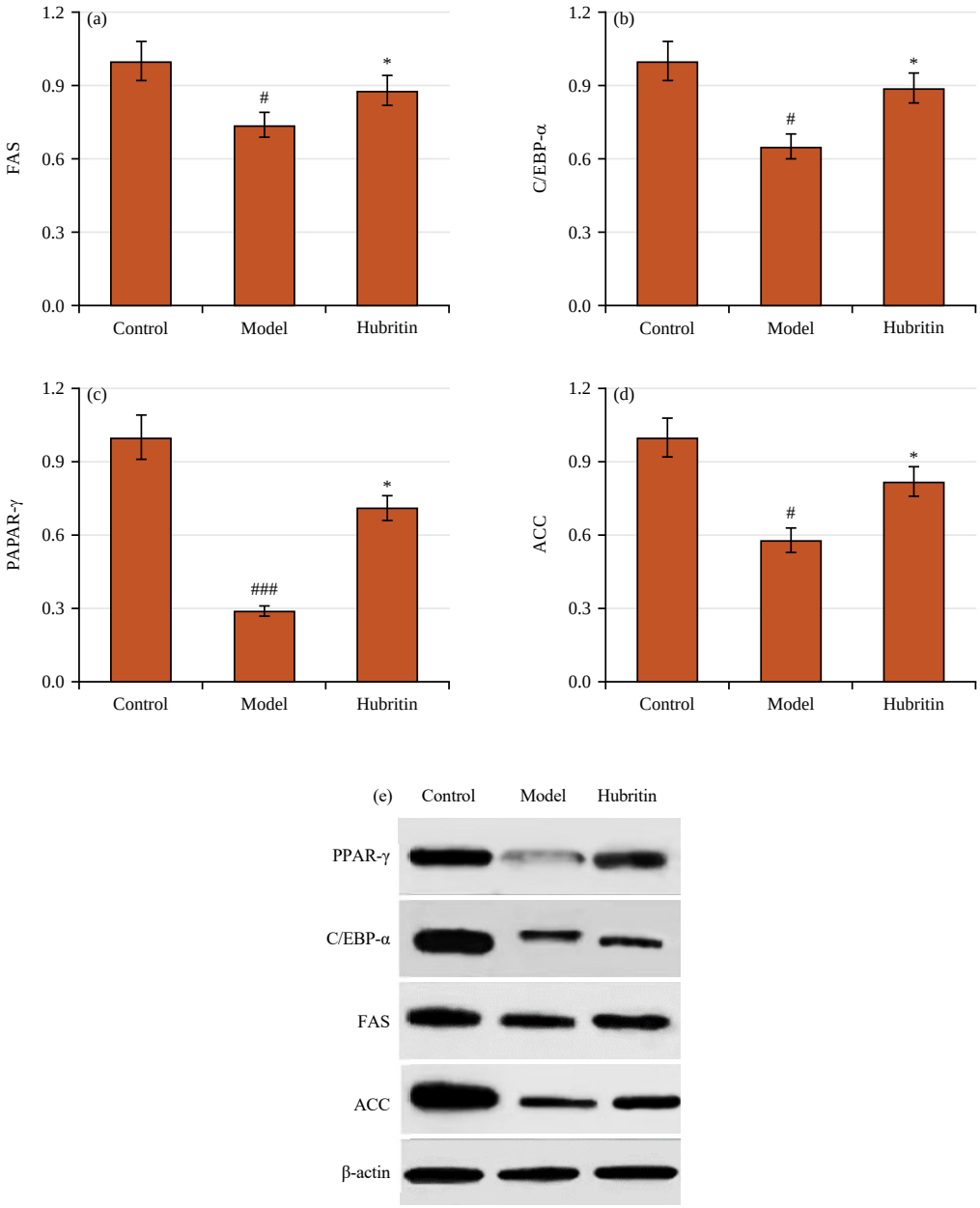

Fig. 9(a-e): Effects of picroside on protein levels of (a) PPAR-γ SPW, (b) PPAR-γ, (c) C/EBP-α, (d) FAS and (e) ACC western blotting results

#Compared with Ctrl group ($p<0.05$), ###Compared with Ctrl group ($p<0.001$) and *Compared with Mod group ($p<0.05$)

DISCUSSION

This study investigated the variation in picroside content under different particle sizes of *Coptis chinensis* roots and rhizomes granules. It was observed that with a decrease in particle size, the extraction yield of picroside increased, indicating better extraction efficiency. This phenomenon may be attributed to the larger surface area of smaller particles, which enhances the effective extraction region, thereby facilitating greater solvent contact, promoting the dissolution and release of picroside. Smaller particles have enhanced contact with the solvent, leading to increased transfer rates and extraction efficiency of the extract. However, using finer particles for reflux extraction may lead to overly concentrated solutions and a higher risk of boiling over[22], thereby increasing the experimental risk. Subsequently, this study evaluated the

differences in the purification effectiveness of picroside using various resin types. Different resin types possess distinct chemical properties and pore structures[23], which may contribute to variations in their adsorption capacities for picroside. The results of this study confirm the performance ranking of macroporous adsorption resins in purifying picroside as follows: D201>AB-8>D101>NKA-9>D3520> DB301>HPD100. Additionally, irrespective of the concentration of ethanol treatment, the resolution rate of picroside by D201 macroporous adsorption resin consistently remained above 80%. The D201 MPAR likely possesses surface characteristics and pore structures that are more suitable for interacting with picroside, leading to enhanced adsorption capacity. On the other hand, HPD100 MPAR might have inferior compatibility, resulting in lower adsorption efficiency[24]. As a results, D201 MPAR exhibited the highest picroside desorption rate, likely due to its strong interaction with picroside molecules, making them more easily released during the desorption process. As ethanol concentration increased, the picroside desorption rate of D201 MPAR showed an initial increase followed by a decrease. This phenomenon could be attributed to the fact that low concentrations of ethanol disrupt the interaction between picroside and the resin, facilitating the desorption process. However, with further increase in ethanol concentration, solvent effects or changes in the reactivity of picroside molecules[25,26] might lead to a decrease in the desorption rate[27].

The GDM is characterized by abnormal glucose metabolism in the maternal body during pregnancy, representing one of the initial occurrences of diabetes and a common complication during pregnancy. Throughout gestation, hormones produced by the placenta and pregnancy-associated hormones induce elevated levels of cholesterol and triglycerides to meet the demands of fetal growth and development[27]. However, in some pregnant women, insufficient insulin secretion or increased insulin resistance can result in elevated blood glucose levels, leading to the onset of gestational diabetes. For women with gestational diabetes, the levels of TC and TG may be slightly higher compared to pregnant women without gestational diabetes[28,29], owing to increased release of fatty acids due to insulin resistance, thereby stimulating the synthesis of cholesterol and triglycerides in the liver[30]. This study discovered that induction of 3T3-L1 cells using DMEM medium containing IBMX, dexamethasone and insulin to prepare a GDM cell model resulted in significantly elevated levels of TC and TG. This indicates abnormal synthesis and accumulation of cholesterol and triglycerides in the cells of the model group, possibly associated with insulin resistance, abnormal glucose metabolism and dysregulation of fatty acid metabolism. These findings aligned with the observed lipid metabolism disorders in other studies on GDM models[31]. Picroside, as a natural herbal component, has been extensively studied for its regulatory effects on lipid metabolism. The present study found that treatment with picroside at different concentrations significantly reduced TC and TG levels in the 3T3-L1 cell model, exhibiting concentration-dependent characteristics. This suggests that picroside may have the potential to regulate fat metabolism.

The LncRNA-MALAT1 is implicated in numerous biological processes and the development of diseases. Its association with GDM occurrence and related pathophysiological mechanisms has been reported by Cremer *et al.*[32]. One study revealed that upregulation of lncRNA-MALAT1 may be associated with adipocyte differentiation and fatty acid synthesis[33]. This suggests a potential role for lncRNA-MALAT1 in regulating fat synthesis processes. Furthermore, another study confirmed a correlation between the expression levels of lncRNA-MALAT1 in samples from adipose tissue, blood or urine and obesity or other metabolic-related diseases[34]. This study observed a significant upregulation of lncRNA-MALAT1 expression in the 3T3-L1 cell model, while treatment with different concentrations of picroside led to a gradual decrease in lncRNA-MALAT1 expression in the 3T3-L1 cell model, exhibiting concentration-dependent characteristics. MicroRNAs (miRNAs) are single-stranded small RNA molecules approximately 21 to 23 nucleotides in length. Most lncRNAs share structural similarities with mRNAs, suggesting that miRNAs may negatively regulate lncRNA expression through mechanisms similar to mRNA regulation, thus exerting biological functions. The LncRNAs competitively bind to the 3'-UTR of target gene mRNAs with miRNAs, indirectly inhibiting the negative regulation of target gene mRNA by miRNAs. The miR-21 may be one of the target mRNAs of lncRNA-MALAT1[35]. Studies have compared the expression levels of miR-21 between patients with GDM and normal pregnant women, revealing significant differences in miR-21 expression levels between GDM patients and normal pregnant women[36]. In GDM, insulin resistance and impaired pancreatic β-cell function are involved. Changes in miR-21 expression may participate in the occurrence of GDM by affecting insulin signal transduction and pancreatic β-cell function. The miR-21 may regulate key genes and signaling pathways during adipocyte differentiation and maturation, thereby affecting the synthesis and storage of fatty acids within adipocytes[37]. Elevated levels of miR-21 expression may be observed in obese and metabolically disturbed individuals, where its

upregulation is associated with abnormal fat storage and lipid metabolism, further influencing the process of fat synthesis. Researchers such as Calo *et al.*[38] found that miR-21 can interfere with fat synthesis processes by targeting molecules such as glucocorticoid receptors, PPAR-γ and its coactivators. This study observed a significant downregulation of miR-21 expression in the 3T3-L1 cell model, while treatment with different concentrations of picroside led to a gradual increase in miR-21 expression in the 3T3-L1 cell model, exhibiting concentration-dependent characteristics. This suggests that picroside may have a regulatory effect on the expression of lncRNA-MALAT1 and miR-21 in GDM.

The PPAR-γ is a nuclear receptor that plays a crucial role in regulating insulin sensitivity in adipose tissue and pancreatic β-cells. In GDM, the activity of PPAR-γ in adipocytes and pancreatic β-cells may be suppressed, leading to insulin resistance. The GDM patients often exhibit increased inflammation and the downregulation of PPAR-γ may be associated with enhanced inflammatory response[39]. The C/EBP-α is a key transcription factor that plays an important role in adipocyte differentiation and function. The expression levels of C/EBP-α are lower in GDM patients, which may inhibit adipocyte differentiation and subsequently affect the process of fat synthesis[40]. The FAS is a key enzyme in fatty acid synthesis and participates in the process of fatty acid synthesis. The expression levels of FAS are lower in GDM patients, which may lead to inhibition of fatty acid synthesis and affect fat synthesis. The ACC is another important regulatory enzyme in fatty acid synthesis[41,42]. The ACC participates in the synthesis of acetyl-CoA, which is a key step in fatty acid synthesis. Lower expression levels of ACC in GDM may lead to reduced synthesis of acetyl-CoA, thereby affecting the process of fat synthesis[43]. This study found that the expression of FAS, C/EBP-α, PPAR-γ and ACC was significantly downregulated in the 3T3-L1 cell model, while treatment with different concentrations of picroside led to a gradual increase in the expression of FAS, C/EBP-α, PPAR-γ and ACC in the 3T3-L1 cell model, exhibiting concentration-dependent characteristics. Picroside may promote the expression of PPAR-γ to restore the process of fat synthesis[44]. Additionally, picroside can regulate adipocyte differentiation and fatty acid synthesis by affecting the PPAR-γ signaling pathway and the expression of related regulatory proteins.

CONCLUSION

The work investigated the role of picroside in GDM fat synthesis and the roles played by lncRNA-MALAT1, miR-21 and PPAR-γ SPW in this process. The outcomes in this work revealed that picroside effectively downregulated of TC, TG and lncRNA-MALAT1 in patients with GDM, while simultaneously upregulating PPAR-γ, C/EBP-α, FAS and ACC. This suggested that picroside regulated the involvement of lncRNA-MALAT1/miR-21/PPAR-γ SPW in fat synthesis of patients with GDM. However, this work also was subjected to some limitations, as it only utilized human subcutaneous adipocytes for experimentation and lacked validation of its findings through animal models or clinical studies. Additionally, it could further explore specific molecular mechanisms and biological processes to deepen the understanding of picroside's role in regulating fat synthesis. Nevertheless, this work presented significant importance for gaining deeper insights into the pathological mechanisms of GDM and identifying new therapeutic strategies. Furthermore, it offered new insights and directions for the application of picroside and related SPW research.

SIGNIFICANCE STATEMENT

This study primarily investigated the regulatory effect of picroside on fat synthesis in Gestational Diabetes Mellitus (GDM) patients and analyzed its role in modulating the lncRNA-MALAT1, miR-21 and PPAR-γ signaling pathways. The results demonstrated that picroside reduced triglyceride and total cholesterol levels in fat cells of GDM through modulation of the lncRNA-MALAT1/miR-21/PPAR-γ signaling pathway, thereby participating in the regulation of fat synthesis. These findings hold significant implications for a deeper understanding of the pathophysiological mechanisms underlying GDM and the exploration of relevant intervention strategies. Subsequent research should further investigate the potential application value of picroside in diabetes treatment and disease management.

REFERENCES

1. Alfadhli, E.M., 2015. Gestational diabetes mellitus. Saudi Med. J., 36: 399-406.
2. Sweeting, A., J. Wong, H.R. Murphy and G.P. Ross, 2022. A clinical update on gestational diabetes mellitus. Endocr. Rev., 43: 763-793.
3. Lende, M. and A. Rijhsinghani, 2020. Gestational diabetes: Overview with emphasis on medical management. Int. J. Environ. Res. Public Health, Vol. 17. 10.3390/ijerph17249573.
4. Rasmussen, L., C.W. Poulsen, U. Kampmann, S.B. Smedegaard, P.G. Ovesen and J. Fuglsang, 2020. Diet and healthy lifestyle in the management of gestational diabetes mellitus. Nutrients, Vol. 12. 10.3390/nu12103050.

5. Johns, E.C., F.C. Denison, J.E. Norman and R.M. Reynolds, 2018. Gestational diabetes mellitus: Mechanisms, treatment, and complications. Trends Endocrinol. Metab., 29: 743-754.
6. Kamana, K.C., S. Shakya and H. Zhang, 2015. Gestational diabetes mellitus and macrosomia: A literature review. Ann. Nutr. Metab., 66: 14-20.
7. Valero, P., G. Fuentes, M. Cornejo, S. Vega and A. Grismaldo *et al*., 2022. Exposome and foetoplacental vascular dysfunction in gestational diabetes mellitus. Mol. Aspects Med., Vol. 87. 10.1016/j.mam.2021.101019.
8. Liu, Y., R. Sun, X. Lin, L. Wu and H. Chen *et al*., 2022. Procyanidins and its metabolites by gut microbiome improves insulin resistance in gestational diabetes mellitus mice model via regulating NF-κB and NLRP3 inflammasome pathway. Biomed. Pharmacother., Vol. 151. 10.1016/j.biopha.2022.113078.
9. Zhou, Y., R. Zhao, Y. Lyu, H. Shi and W. Ye *et al*., 2021. Serum and amniotic fluid metabolic profile changes in response to gestational diabetes mellitus and the association with maternal-fetal outcomes. Nutrients, Vol. 13. 10.3390/nu13103644.
10. Liu, Y., B. Wang, S. Shu, Z. Li and C. Song *et al*., 2021. Analysis of the *Coptis chinensis* genome reveals the diversification of protoberberine-type alkaloids. Nat. Commun., Vol. 12. 10.1038/s41467-021-23611-0.
11. Chen, Q., R. Ren, Q. Zhang, J. Wu and Y. Zhang *et al*., 2021. *Coptis chinensis* Franch polysaccharides provide a dynamically regulation on intestinal microenvironment, based on the intestinal flora and mucosal immunity. J. Ethnopharmacol., Vol. 267. 10.1016/j.jep.2020.113542.
12. Li, T., L. Xu, R. Zheng, X. Wang, L. Li, H. Ji and Q. Hu, 2020. Picroside II protects against cholestatic liver injury possibly through activation of farnesoid X receptor. Phytomedicine, Vol. 68. 10.1016/j.phymed.2019.153153.
13. Piao, X., X. Sui, B. Liu, T. Cui and Z. Qi, 2021. Picroside II improves severe acute pancreatitis-induced hepatocellular injury in rats by affecting JAK2/STAT3 phosphorylation signaling. BioMed Res. Int., Vol. 2021. 10.1155/2021/9945149.
14. Ma, S., X. Wang, F. Lai and C. Lou, 2020. The beneficial pharmacological effects and potential mechanisms of picroside II: Evidence of its benefits from *in vitro* and *in vivo*. Biomed. Pharmacother., Vol. 130. 10.1016/j.biopha.2020.110421.
15. Piao, X., B. Liu, X. Sui, S. Li and W. Niu *et al*., 2020. Picroside II improves severe acute pancreatitis-induced intestinal barrier injury by inactivating oxidative and inflammatory TLR4-dependent PI3K/AKT/NF-κB signaling and improving gut microbiota. Oxid. Med. Cell. Longevity, Vol. 2020. 10.1155/2020/3589497.
16. Yang, X., W. Gao, B. Wang, X. Wang and H. Guo *et al*., 2017. Picroside II inhibits RANKL-mediated osteoclastogenesis by attenuating the NF-κB and MAPKs signaling pathway *in vitro* and prevents bone loss in lipopolysaccharide treatment mice. J. Cell. Biochem., 118: 4479-4486.
17. Li, H., W. Du, Y. Yuan, J. Xue, Q. Li and L. Wang, 2022. The protective effect of picroside II on isoflurane-induced neuronal injury in rats via downregulating miR-195. Neuroimmunomodulation, 29: 202-210.
18. Dhami-Shah, H., R. Vaidya, M. Talwadekar, E. Shaw, S. Udipi, U. Kolthur-Seetharam and A.D.B. Vaidya, 2021. Intervention by picroside II on FFAs induced lipid accumulation and lipotoxicity in HepG2 cells. J. Ayurveda Integr. Med., 12: 465-473.
19. Qin, Z., W. Wang, D. Liao, X. Wu and X. Li, 2018. UPLC-Q/TOF-MS-based serum metabolomics reveals hypoglycemic effects of *Rehmannia glutinosa*, *Coptis chinensis* and their combination on high-fat-diet-induced diabetes in KK-Ay mice. Int. J. Mol. Sci., Vol. 19. 10.3390/ijms19123984.
20. Wang, Y., Y.R. Mo, J. Tan, L.X. Wu, Y. Pan and X.D. Chen, 2022. Effects of growing *Coptis chinensis* Franch in the natural understory *vs*. under a manmade scaffold on its growth, alkaloid contents, and rhizosphere soil microenvironment. PeerJ, Vol. 10. 10.7717/peerj.13676.
21. Li, Q., M. Wang, X. Yuan, D. Li and H. Xu *et al*., 2021. Study on the adsorption and desorption performance of magnetic resin for Congo red. Environ. Technol., 42: 1552-1559.
22. Cheng, C., R. Guo, J. Lan and S. Jiang, 2017. Extraction of lotus fibres from lotus stems under microwave irradiation. R. Soc. Open Sci., Vol. 4. 10.1098/rsos.170747.
23. Tang, B., X. Chen, P. Laborda and F. Liu, 2021. Efficient direct preparation of antifungal alteramide B from *Lysobacter enzymogenes* fermentation broth by macroporous resin adsorption. Bioresour. Technol., Vol. 319. 10.1016/j.biortech.2020.124220.
24. Venkiteshwaran, K., E. Wells and B.K. Mayer, 2020. Kinetics, affinity, thermodynamics, and selectivity of phosphate removal using immobilized phosphate-binding proteins. Environ. Sci. Technol., 54: 10885-10894.
25. Niphadkar, S.S. and V.K. Rathod, 2017. Adsorption kinetics, isotherm, and thermodynamics studies of acetyl-11-keto-β-boswellic acids (AKBA) from *Boswellia serrata* extract using macroporous resin. Prep. Biochem. Biotechnol., 47: 804-812.
26. Marin, N.M. and I. Stanculescu, 2021. Application of amberlite IRA 402 resin adsorption and laccase treatment for acid blue 113 removal from aqueous media. Polymers, Vol. 13. 10.3390/polym13223991.
27. Lanjekar, K.J. and V.K. Rathod, 2024. Recovery and separation of glycyrrhizic acid from natural deep eutectic solvent (NADES) extract by macroporous resin: Adsorption kinetics and isotherm studies. Prep. Biochem. Biotechnol., 54: 39-48.

28. Cho, Y., Y. Chang, S. Ryu, S.H. Wild and C.D. Byrne, 2023. Synergistic effect of non-alcoholic fatty liver disease and history of gestational diabetes to increase risk of type 2 diabetes. Eur. J. Epidemiol., 38: 901-911.
29. Xu, W., M. Tang, J. Wang and L. Wang, 2020. Anti-inflammatory activities of puerarin in high-fat diet-fed rats with streptozotocin-induced gestational diabetes mellitus. Mol. Biol. Rep., 47: 7537-7546.
30. Karasek, D., V. Kubickova, O. Krystynik, D. Goldmannova, L. Cibickova and J. Schovanek, 2020. Circulating levels of selected adipokines in women with gestational diabetes and type 2 diabetes. J. Appl. Biomed., 18: 54-60.
31. Song, X., C. Wang, T. Wang, S. Zhang and J. Qin, 2023. Obesity and risk of gestational diabetes mellitus: A two-sample Mendelian randomization study. Diabetes Res. Clin. Pract., Vol. 197. 10.1016/j.diabres.2023.110561.
32. Cremer, S., K.M. Michalik, A. Fischer, L. Pfisterer and N. Jaé *et al*., 2019. Hematopoietic deficiency of the long noncoding RNA MALAT1 promotes atherosclerosis and plaque inflammation. Circulation, 139: 1320-1334.
33. Li, H., Q. Zhao, L. Chang, C. Wei and H. Bei *et al*., 2019. LncRNA MALAT1 modulates ox-LDL induced EndMT through the Wnt/β-catenin signaling pathway. Lipids Health Dis., Vol. 18. 10.1186/s12944-019-1006-7.
34. Liu, S.X., F. Zheng, K.L. Xie, M.R. Xie, L.J. Jiang and Y. Cai, 2019. Exercise reduces insulin resistance in type 2 diabetes mellitus via mediating the lncRNA MALAT1/microRNA-382-3p/resistin axis. Mol. Ther. Nucleic Acids, 18: 34-44.
35. Huang, B., X. Guo and Y. Li, 2020. lncRNA MALAT1 regulates the expression level of miR-21 and interferes with the biological behavior of colon cancer cells. J. BUON, 25: 907-913.
36. Chartoumpekis, D.V., A. Zaravinos, P.G. Ziros, R.P. Iskrenova, A.I. Psyrogiannis, V.E. Kyriazopoulou and I.G. Habeos, 2012. Differential expression of microRNAs in adipose tissue after long-term high-fat diet-induced obesity in mice. PLoS ONE, Vol. 7. 10.1371/journal.pone.0034872.
37. Xia, L., Z. Zhao, X. Yu, C. Lu and P. Jiang *et al*., 2021. Integrative analysis of miRNAs and mRNAs revealed regulation of lipid metabolism in dairy cattle. Funct. Integr. Genomics, 21: 393-404.
38. Calo, N., P. Ramadori, C. Sobolewski, Y. Romero and C. Maeder *et al*., 2016. Stress-activated *miR-21/miR-21** in hepatocytes promotes lipid and glucose metabolic disorders associated with high-fat diet consumption. Gut, 65: 1871-1881.
39. Lu, J., D. Wang, B. Ma, X. Gai, X. Kang, J. Wang and K. Xiong, 2022. Blood retinol and retinol-binding protein concentrations are associated with diabetes: A systematic review and meta-analysis of observational studies. Eur. J. Nutr., 61: 3315-3326.
40. Tian, H., J. Luo, P. Guo, C. Li and X. Zhang, 2023. C/EBPα promotes triacylglycerol synthesis via regulating *PPARG* promoter activity in goat mammary epithelial cells. J. Anim. Sci., Vol. 101. 10.1093/jas/skac412.
41. Su, K., B. Yi, B.Q. Yao, T. Xia, Y.F. Yang, Z.H. Zhang and C. Chen, 2020. Liraglutide attenuates renal tubular ectopic lipid deposition in rats with diabetic nephropathy by inhibiting lipid synthesis and promoting lipolysis. Pharmacol. Res., Vol. 156. 10.1016/j.phrs.2020.104778.
42. Seo, Y.J., K.J. Kim, J. Choi, E.J. Koh and B.Y. Lee, 2018. *Spirulina maxima* extract reduces obesity through suppression of adipogenesis and activation of browning in 3T3-L1 cells and high-fat diet-induced obese mice. Nutrients, Vol. 10. 10.3390/nu10060712.
43. Bates, J., A. Vijayakumar, S. Ghoshal, B. Marchand and S. Yi *et al*., 2020. Acetyl-CoA carboxylase inhibition disrupts metabolic reprogramming during hepatic stellate cell activation. J. Hepatol., 73: 896-905.
44. Adibi, J.J., J.P. Buckley, M.K. Lee, P.L. Williams and A.C. Just *et al*., 2017. Maternal urinary phthalates and sex-specific placental mRNA levels in an urban birth cohort. Environ. Health, Vol. 16. 10.1186/s12940-017-0241-5.